COUPLED THERMO-MECHANICAL ANALYSES OF DYNAMICALLY LOADED RUBBER CYLINDERS[1]

Arthur R. Johnson and Tzi-Kang Chen
Army Research Laboratory, MS 240
Analytical and Computational Methods Branch
NASA Langley Research Center
Hampton, VA 23681-0001

ABSTRACT

A procedure that models coupled thermo-mechanical deformations of viscoelastic rubber cylinders by employing the ABAQUS finite element code is described. Computational simulations of hysteretic heating are presented for several tall and short rubber cylinders both with and without a steel disk at their centers. The cylinders are compressed axially and are then cyclically loaded about the compressed state. The non-uniform hysteretic heating of the rubber cylinders containing a steel disk is presented. The analyses performed suggest that the coupling procedure should be considered for further development as a design tool for rubber degradation studies.

KEY WORDS: Viscoelasticity, Structural Analysis, Thermal Analysis

1. INTRODUCTION

1.1 Background Rubber is employed to carry large loads in tires, gaskets, and tank track pads. It is also used to provide damping and system stability in complex mechanical systems such as helicopter rotors. In these applications, the rubber is typically stiffened by the addition of carbon black. The filled rubber tends to be a poor conductor of heat, yet it also exhibits very large hysteretic energy loss during cyclic loading. Also, the mechanical properties of rubber are strongly dependent on temperature. Faced with the above issues, designers interested in modeling the detailed response of complex-shaped rubber components need to be able to compute the coupled thermo-mechanical behavior of rubber.

An example of the importance of understanding the thermo-mechanical response of filled rubber is given in a series of papers presented at the "Thirty Second Sagamore Army Materials Research Conference" held a Lake Luzerne, NY in 1985 (1-4). In these papers, hysteretic heating, thermo-

[1]This paper is declared a work of the U.S. Government and is not subject to copyright protection in the United States.

mechanical degradation, and fatigue of rubber-coated road wheels and tank track pads are all discussed. Uncoupled thermo-mechanical finite element analyses, and sensitivity studies were conducted with finite element codes. It was observed that the viscoelastic properties and the shape of the rubber solid are the most important factors in determining temperature rise (1). The degradation studies indicate that the failure of cyclically loaded "rubber-like" polyurethane blocks depends on the hard segment transition temperature (2). Experiments were conducted which proved that the large strain hysteretic heating rate does not correlate with the heating rates predicted using the popular complex modulus material data (3). Also determined is the fact that failure under cyclic loading can be "significantly different from that obtained in constant rate testing" (4). These conclusions suggest that detailed computational simulations of large strain dynamic loading of rubber-like solids, performed as part of a material degradation study, require accurate modeling of the large strain viscoelastic properties and a coupling of the mechanical and thermal models.

The purpose of this work is to establish and test a computational tool for analyzing hysteretic heating in rubber components. In this paper, large deformation rubber viscoelasticity and heat transfer finite element models are coupled and employed to computationally simulate the hysteretic heating of dynamically loaded rubber cylinders.

The formulations for large strain rubber viscoelasticity and heat transfer employed in ABAQUS are outlined below to facilitate the description of the thermo-mechanical coupling performed in this study. Detailed information on these two formulations and their finite element implementation is available in the ABAQUS Theory Manual (5). Additional information on formulations for rubber viscoelasticity are available in the literature (6-10). Only moderate temperature changes were simulated in this study, so time-temperature superposition is not discussed.

1.2 Rubber Viscoelasticity The virtual work statement, without inertial effects included, for a solid of volume V and surface area S is:

$$dW_I = \int_V \mathbf{s} : d\mathbf{D}_\mathbf{v}\, dV = \int_S d\mathbf{v}^T \mathbf{t}\, dS + \int_V d\mathbf{v}^T \mathbf{f}\, dV \qquad [1]$$

where dW_I is the internal energy due to the virtual displacement $d\mathbf{v}$, $\mathbf{s}$ is the Cauchy stress, $d\mathbf{D}_\mathbf{v}$ is the virtual rate of deformation, $\mathbf{t}$ is the traction stress vector acting on S, and $\mathbf{f}$ is the body force vector acting within V. Details on the notation used below are given in the Appendix. Equation [1] is used to build the mechanical finite element equilibrium equations. The following details describe how the viscoelastic behavior of rubber is approximated. In the reference configuration, the strain energy part of Equation [1] is written:

$$dW_I = \int_{V_0} J\mathbf{s} : d\mathbf{D}_\mathbf{v}\, dV_0 \qquad [2]$$

where V_0 is the volume V in its reference state. When the solid is rubber, Equation [2] is expressed as:

$$dW_I = \int_{V_0} \left\{ 2\left[\left(\frac{\partial U}{\partial \bar{I}_1} + \bar{I}_1 \frac{\partial U}{\partial \bar{I}_2} \right) \overline{\mathbf{B}} - \frac{\partial U}{\partial \bar{I}_2} \overline{\mathbf{B}}^2 \right] : d\mathbf{e} + J \frac{\partial U}{\partial J} de^{vol} \right\} dV_0 \qquad [3]$$

where U is the solid's strain energy density function. In this effort, a standard polynomial form of the rubber's strain energy density was employed as follows:

$$U = \sum_{i+j=1}^{N} C_{ij} \left(\bar{I}_1 - 3\right)^i \left(\bar{I}_2 - 3\right)^j + \sum_{i=1}^{N} \frac{1}{D_i} \left(\frac{1}{\left(1 + e_{th}\right)^3} - 1 \right)^{2i} \qquad [4]$$

where the constants C_{ij} and D_i are determined from measured stress-strain data, and e_{th} is the thermal expansion strain. A history integral method is employed in ABAQUS to model viscoelastic material behavior. In the viscoelasticity formulation the material constants in the strain energy density function are made time dependent as follows:

$$C_{ij}(t) = C_{ij}^0 \left(1 - \sum_{\ell=1}^{n} \bar{g}_\ell \left(1 - e^{-\frac{t}{t_\ell}} \right) \right) \quad \text{and} \quad \frac{1}{D_i(t)} = \frac{1}{D_i^0} \left(1 - \sum_{\ell=1}^{n} \bar{k}_\ell \left(1 - e^{-\frac{t}{t_\ell}} \right) \right) \qquad [5]$$

where the constants $\bar{g}_\ell$, $\bar{k}_\ell$, and t_ℓ are determined by fitting the analytical form of relaxation stresses to experimental data (5, 9-12), the constants C_{ij}^0 and D_i^0 are the "elastic" constants, mention above in Equation [4], determined from high strain rate loading tests, and the superscript 0 refers to the material's instantaneous response.

1.3 Heat Transfer. The variational statement of the energy balance equation for heat transfer, together with Fourier's law, for a deformed solid of volume V, and surface area S is:

$$\int_V r \frac{dU_q}{dt} dq \, dV + \int_V \frac{\partial dq}{\partial \mathbf{x}} \mathbf{k} \frac{\partial q}{\partial \mathbf{x}} dV = \int_V dq \, r \, dV + \int_S dq \, q \, dS \qquad [6]$$

where q is the temperature, U_q is the internal thermal energy, r is the density, q is the heat flux per unit area, r is the heat supplied per unit volume, $\mathbf{k}$ is a conductivity matrix, and dq is a virtual temperature field satisfying the essential boundary conditions. Equation [6] is used to build the transient heat transfer finite element equations.

2. COUPLED THERMO-MECHANICAL MODEL

Finite element discretization of the mechanical and thermal variational statements, Equations [1] and [6], results in systems of time dependent mechanical and thermal differential equations. For the variational statements given above, the only thermo-mechanical coupling that exists is through the thermal expansion strain, e_{th}. Additional thermo-mechanical coupling can be approximated by computing the rate of viscoelastic energy dissipation from the mechanical equations and inputting that rate into the thermal equations. ABAQUS internally computes and stores a running total of the energy dissipated as a function of time. Internal variables can be

employed to compute the energy dissipation rate from this running total and pass it on to the thermal analysis.

2.1 Element The eight-node hybrid axisymmetric CAX8RHT element in ABAQUS was utilized for the examples given below. The element uses biquadratic displacement interpolation, and bilinear temperature and pressure interpolation. It also employs reduced integration (see Figure 1.)

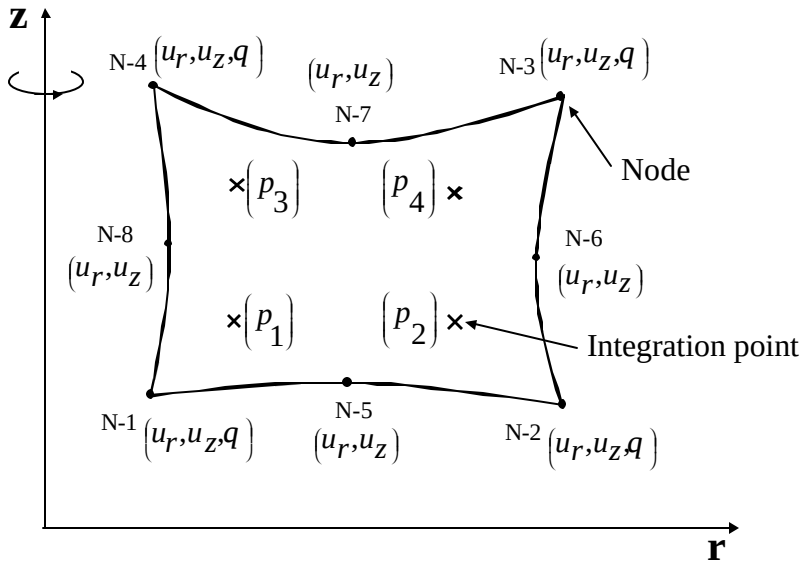

Figure 1. Axisymmetric CAX8RHT element.

The variables employed in the thermal element are the temperatures, q, at the four corner nodes. The stress element has radial, u_r, and axial, u_z, displacements at the eight nodes and hydrostatic pressure, p_i, variables at each of the four integration points. Heating rates are applied at the four integration points.

2.2 Coupling Procedure Two internal variables are introduced at each of the four integration points in the element. When convergence is achieved, at the end of a time increment, the energy dissipated during the time increment is computed internally (for each integration point in each element) by ABAQUS. The increment is added to and stored as a running total at each integration point. The "user subroutine" option in ABAQUS was employed with the two internal variables to compute the energy dissipation rate and input the rate to the thermal analysis. At each integration point, one internal variable stores the "running total" dissipated energy at the beginning of the time interval. These stored values are used with the ABAQUS "running totals" at the end of the time interval to compute the rates of energy dissipation across the time interval at each integration point. The rate of energy dissipation is stored as the second internal variable and is sent forward to the next time interval to serve as a heating rate in the thermal analysis.

2.3 Cylinder Dimensions, Material Properties, and Loading To investigate the application of the procedure described above, eight cylinders were analyzed for hysteretic heating. Only moderate temperature changes were being simulated so the elastic material constants were not

treated as temperature dependent. Having the elastic constants independent of temperature simplified the calculations presented in this effort, but it is not a limitation of the algorithm.

2.3.1 Dimensions There were two groups of four cylinders each. One group consisted of uniform cylinders and the other group had steel disks at their centers, see Figure 2. All cylinders had the radius, $R = 0.0282\,m$. There were four cylinder heights in each group. The heights were $H = 0.05\,m, 0.0375\,m, 0.025\,m, 0.0125\,m$ respectively. The cylinders were compressed between steel fixtures. The model simulates the case when a lubricant maintains the fixture-rubber interface as frictionless. The internal steel disks were completely attached (bonded) to the rubber. The height and radius of the disks were $0.0025\,m$, and $0.0141\,m$, respectively.

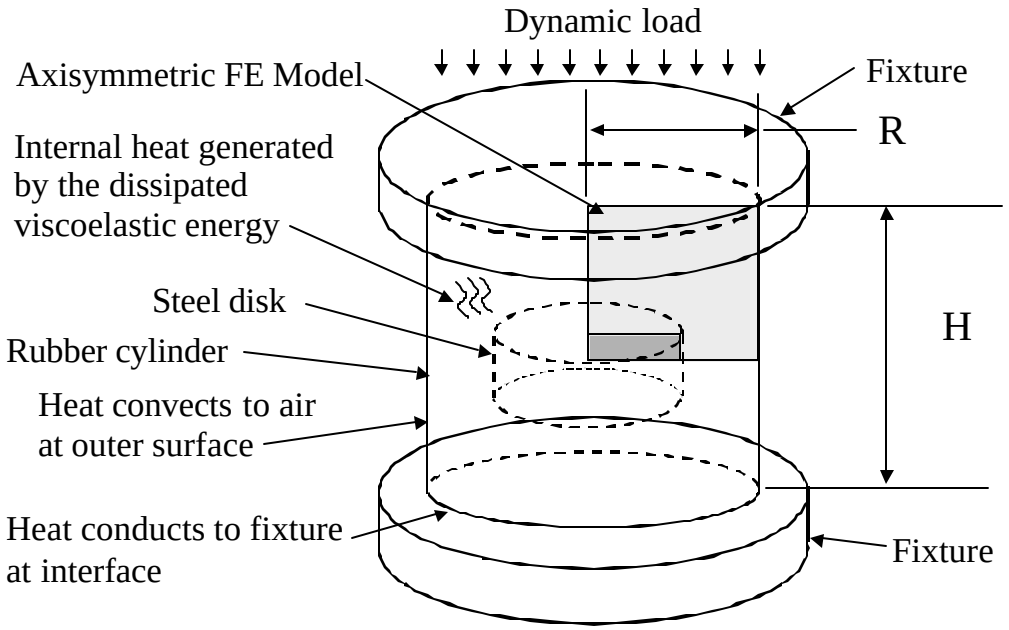

Figure 2. Rubber cylinder, finite element mesh, fixture, and steel disk.

2.3.2 Rubber Properties The rubber energy density was modeled with a two-term Mooney-Rivlin (6) expansion and with two terms in each Prony series (see Equations [4] and [5]). The material constants employed are representative of a soft rubber and are listed below (13)-(15).

The viscoelastic constants are:

$C_{10}^0 = 454545.45\,Pa,\ C_{01}^0 = 45454.54\,Pa,$ and $D_1^0 = 6.667 * 10^{-10}\,Pa^{-1}$

$\overline{g}_1 = 0.2,\ \overline{k}_1 = 0.2,\ t_1 = 0.2\,s$

and $\overline{g}_2 = 0.2,\ \overline{k}_2 = 0.2, t_2 = 1.0\,s$

The thermal material constants are:

Conductivity	$k = 0.20934\ \ J/\left(^\circ C\ m\,\mathrm{s}\right)$
Density	$r = 1000.\ \ kg/m^3$
Specific heat	$\mathrm{c} = 2093.4\ \ J/\left(kg\ ^\circ C\right)$
Expansion	$a = 80. * 10^{-6}\left(^\circ C\right)^{-1}$

The film heat transfer coefficients for the rubber-air and rubber-steel interfaces are $h_A = 5.44284 J/(^\circ C\, m\, s)$ and $h_S = 20934\ J/(^\circ C\, m\, s)$, respectively.

2.3.3 Steel Properties

The elastic constants are:

Young's modulus	$E = 206.8\ GPa$
Poisson's Ratio	$n = 0.3$

The thermal constants are:

Conductivity	$k = 45.83379\ \ J/(^\circ C\, m\, \sec)$
Density	$r = 7849.\ kg/m^3$
Specific heat	$c = 460.\ J/(kg\ ^\circ C)$
Expansion	$a = 12.*10^{-6}(^\circ C)$

2.3.4 Loading Each cylinder was subjected to a constant compressive load with a superimposed cyclic load of sufficient magnitude to produce large strain hysteresis. The loading was:

$$f(t) = -2100 - 1400\ \sin(40.84\,t)\ \text{N} \qquad [7]$$

where t is the time in seconds. The maximum deformation of the tall ($H = 0.05\,m$) uniform cylinder after 130 cycles is shown in Figure 3. The mesh refinement near the top and outer edges is to accommodate the heat transfer gradients at those locations.

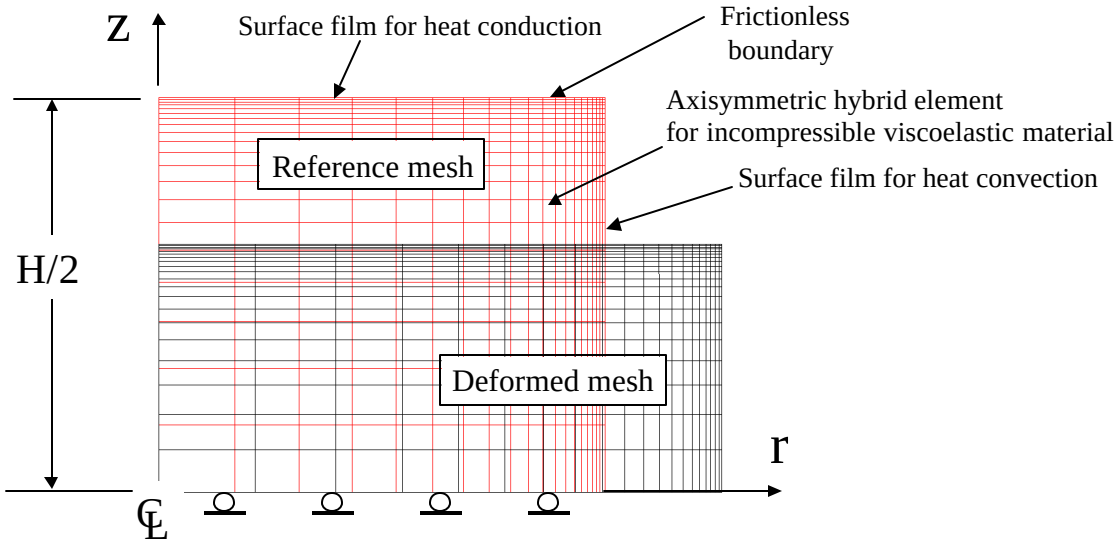

Figure 3. Deformation of a tall uniform cylinder (H = 0.05 m).

The loading and the displacement of the top of the cylinder are shown in Figure 4 for a time interval of 1.0 s. As expected, the displacement curve demonstrates viscoelastic softening or "cyclic creep."

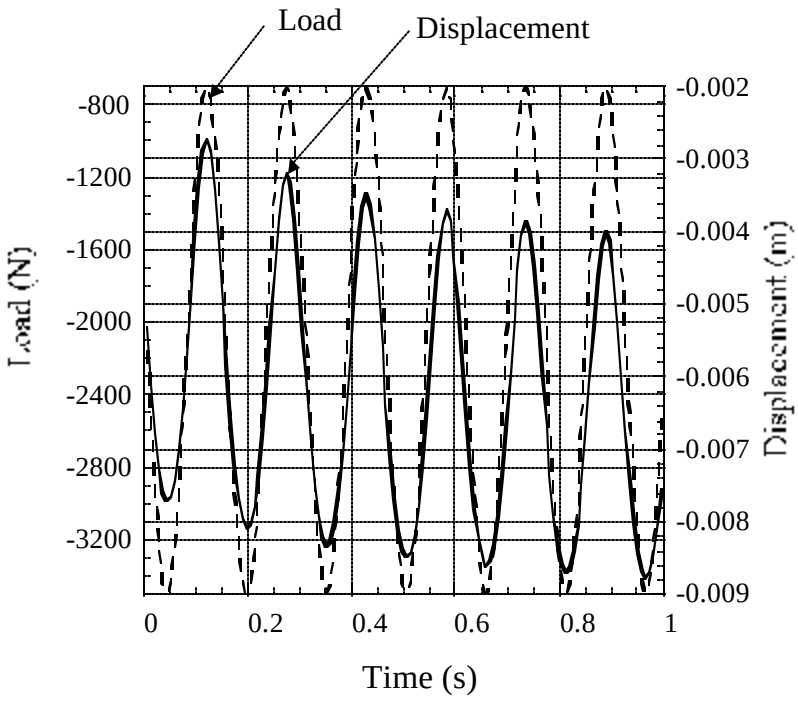

Figure 4. Viscoelastic softening of a tall uniform cylinder (H = 0.05 m).

3. COMPUTED TEMPERATURE DISTRIBUTIONS

A number of analyses were performed to evaluate the nonlinear elastic, the viscoelastic, and the transient heat transfer finite element algorithms separately. Hand calculations and finite difference calculations verified that the algorithms functioned correctly. In the preliminary calculations, the coupling procedure was used with properties representative of track pad materials and the rate at which the temperature increased was similar to rates measured for tests on track pad materials (2). The thermal boundary conditions did not significantly affect the temperature fields computed. The following analyses were performed, employing the coupling procedure described above, to investigate the heating of soft rubber cylinders undergoing large strain dynamic deformations.

3.1 Uniform Cylinders The cyclic load given by Equation [7] was applied to the four uniform cylinders described above. The temperatures, at the center of the cylinders as a function of time for the first 20 s of loading are presented in Figure 5. The frictionless rubber-fixture surface allows the strains to be uniform in the cylinder. Rubber is a poor conductor of heat and the fact that the cylinders heated nearly uniformly regardless of shape (tall or short) was expected.

3.2 Cylinders Containing a Disk It is difficult to estimate hysteretic heating in rubber solids of complex shape because coupled thermo-mechanical analyses are needed in regions of high strain gradients. The group of cylinders containing disks were cyclically loaded to observe the ability of the coupling procedure to predict the distribution of viscoelastic heating in a rubber solid with high strain gradients. The results obtained are reasonable. Figure 6 shows the meshes on the

reference and deformed shapes for the tall cylinder. The temperature distribution in the tall block after 20 s of dynamic loading is shown in Figure 7. Temperatures at points A, B, C, and D in Figure 7 are plotted as a function of time in Figure 8. The outer radial end of the internal disk (point C) is predicted to heat much faster than the rest of the cylinder. Small oscillations in the computed heating rates were observed in these computations. The cause of these oscillations has not been determined.

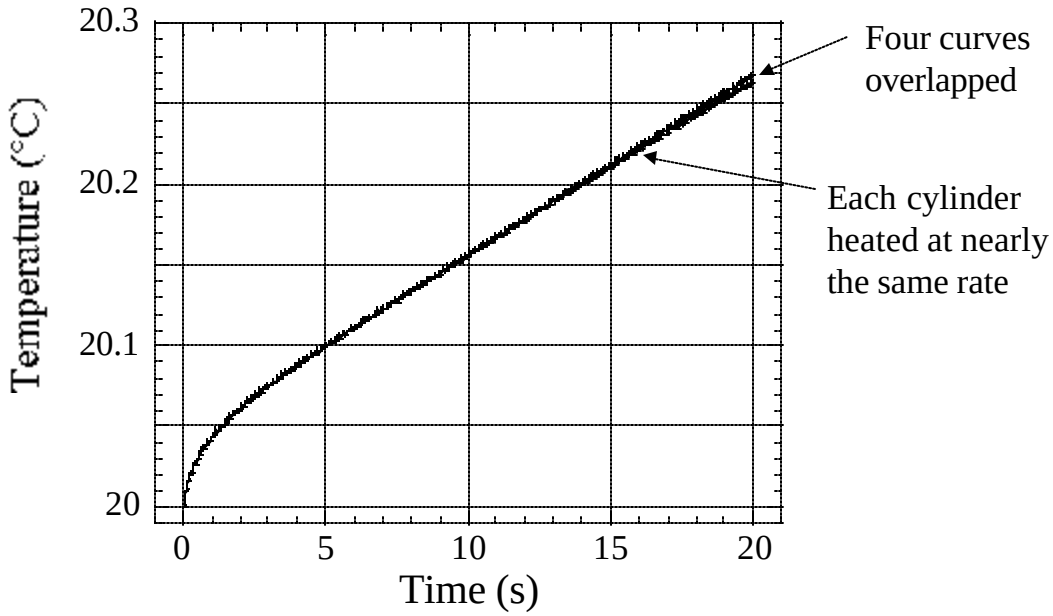

Figure 5. Temperature as a function of time at the center of each uniform cylinder.

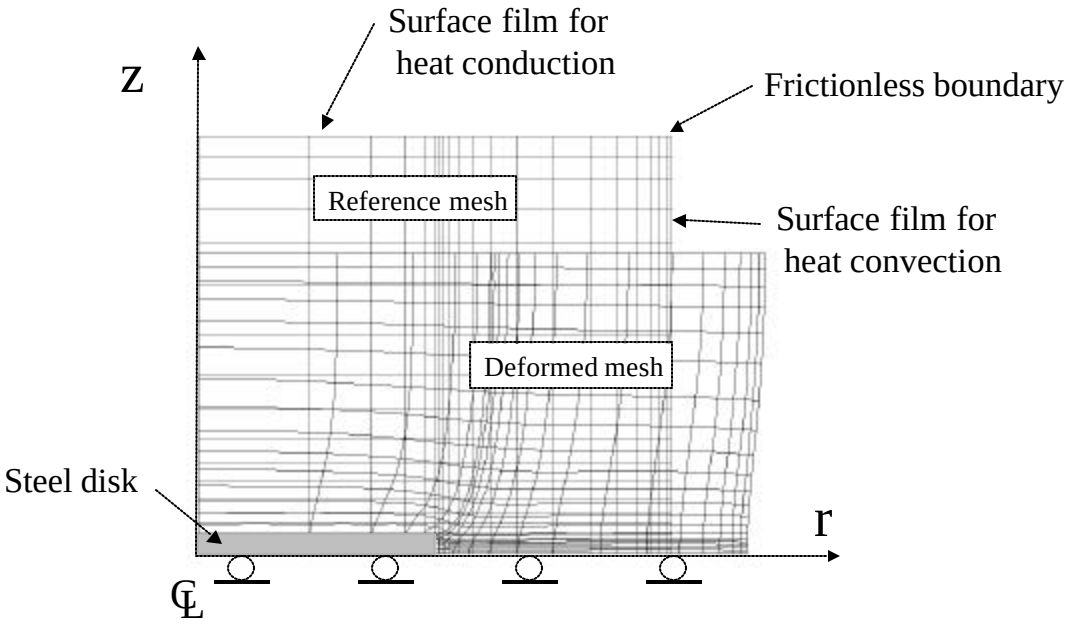

Figure 6. Deformation of a tall cylinder with an internal disk (H = 0.05 m).

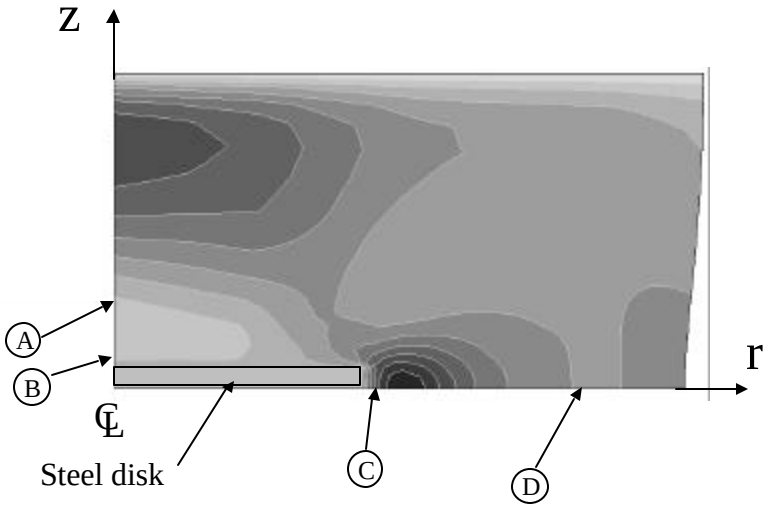

Figure 7. Temperature distribution in a tall cylinder with an internal disk (H = 0.05 m).

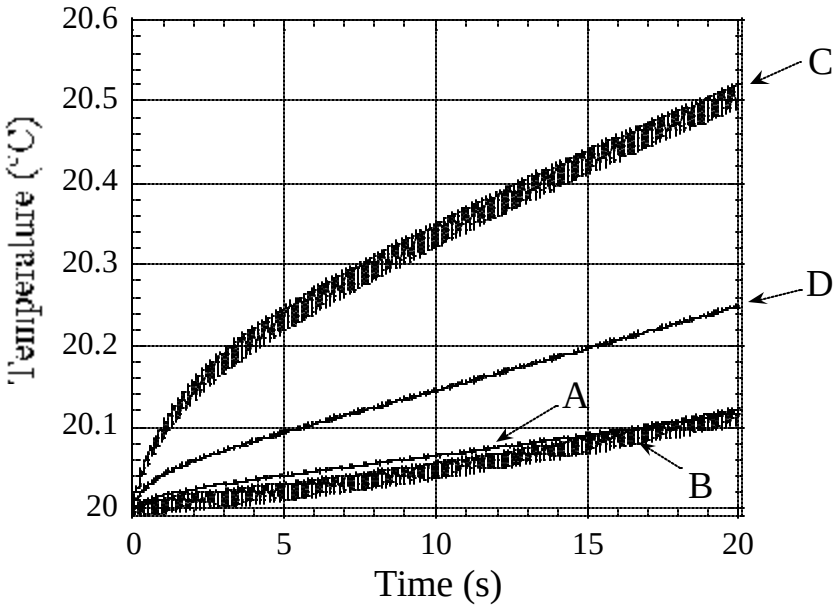

Figure 8. Temperature as a function of time for a tall cylinder with an internal disk (H = 0.05m).

The results were similar for the shorter cylinders. The temperature distribution in the shortest cylinder is presented in Figure 9. As in the case of the tall cylinder, the region of high strain gradient located near the outer radial end of the internal disk (point C) has the most rapid rise in temperature (see Figure 10.)

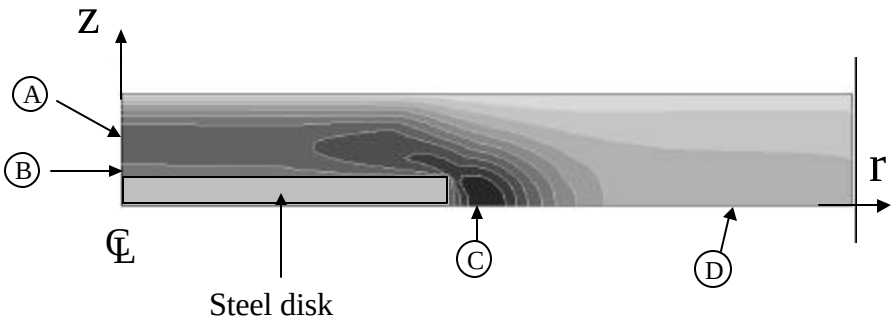

Figure 9. Temperature distribution in a short cylinder with an internal disk (H = 0.0125 m).

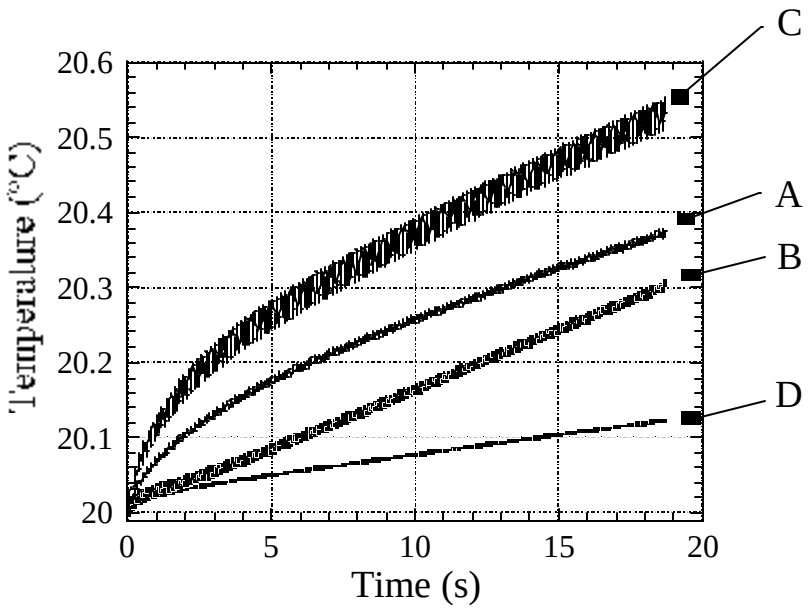

Figure 10. Temperature as a function of time for a short cylinder with an internal disk (H = 0.0125 m).

4. CONCLUSIONS

Accurate predictions of the strain and temperature distributions in rubber components, employed in dynamically loaded structures, are required to perform degradation studies. A procedure which couples a viscoelastic stress analysis with a heat transfer analysis was described. The ABAQUS finite element code was employed to demonstrate the procedure. Both the stress and the thermal analyses are valid for large strains and displacements. A user subroutine was written to track dissipation of energy across time intervals and determine heating rates. The heating rate data is passed forward one time interval in the procedure.

The thermo-mechanical heating of tall and short uniform rubber cylinders (without internal disks) was computed with the coupling procedure. The viscoelastic material properties employed are valid for large strain deformations of soft rubber. The time dependent strains in the cylinders were uniform, and uniform heating was computed.

The thermo-mechanical heating of tall and short rubber cylinders with internal steel disks was also studied. The internal steel disks provided high strain gradients within the rubber cylinders and nonuniform hysteretic heating is observed.

The analyses performed suggest that the coupling procedure should be considered for further development as a design tool for rubber degradation studies. An integrated effort in which the large strain viscoelastic material properties, the heat transfer properties, and the heating rates due to cyclic loading are all determined is recommended.

5. REFERENCES

1. Lesuer, D. R., Goldberg, A., and Patt, J., in Elastomers and Rubber Technology, Eds. R. E. Singler and C. A. Byrne, Library of Congress 86-600600, pp. 211 - 228.
2. Mead, J. L., Singh, S., Roylance, D. K., and Patt, J., in Elastomers and Rubber Technology, Eds. R. E. Singler and C. A. Byrne, Library of Congress 86-600600, pp. 251 - 268.
3. Mead, J. L., and Pattie, E. R., in Elastomers and Rubber Technology, Eds. R. E. Singler and C. A. Byrne, Library of Congress 86-600600, pp. 273 - 280.
4. McKenna, G. B., Bullman, G. W., Flynn, K. M., and Patt, J., in Elastomers and Rubber Technology, Eds. R. E. Singler and C. A. Byrne, Library of Congress 86-600600, pp. 525 - 534.
5. ABAQUS Theory Manual, Version 5.8, Hibbitt, Karlsson & Sorensen Inc., 1080 Main St., Pawtucket, RI, 02860.
6. Ward, I. M., Mechanical Properties of Solid Polymers, John Wiley and Sons, 1983.
7. Malvern, L. E., Introduction to the Mechanics of a Continuous Medium, Prentice-Hall, 1969.
8. Ogden, R. W., Non-Linear Elastic Deformations, Ellis Horwood Limited, 1984.
9. Johnson, A. R., Quigley, C. J., and Mead, J. L., Rubber Chemistry and Technology, 67(5), 904 (1994).
10. Quigley, C. J., Mead, J., and Johnson, A. R., Rubber Chemistry and Technology, 68(1), 230 (1995).
11. Hill, S. A., NASA TM-108394, February 1993.
12. Chen, T., NASA TM-2000-210213 (ARL-TR-2206), May 2000.
13. http://bvsd.k12.co.us/schools/BHS/science/physics/reference/measured/measured.html
14. Clark, S. K. and Dodge, R. N., NASA Contractor Report 3629, 1982.
15. Pitts, D. R. and Sissom, L. E., Heat Transfer, McGraw-Hill Book Co. Library of Congress 77-20255.

APPENDIX

The following notation is included to assist the reader with the description of the ABAQUS finite element algorithm for rubber viscoelasticity.

$X_i \ (i = 1,2,3)$	coordinates of a material point in the reference configuration.
$x_i \ (i = 1,2,3)$	coordinates of a material point in the deformed configuration.
$\mathbf{x} = \mathbf{x}(\mathbf{X}, \mathrm{t})$	vector mapping between the reference and deformed configurations.
$\mathbf{F} = \dfrac{\partial \mathbf{x}}{\partial \mathbf{X}}$	deformation gradient.
$J = \det(\mathbf{F})$	determinate of $\mathbf{F}$ which measures volume change.
$\overline{\mathbf{F}} = J^{-\frac{1}{3}}\mathbf{F}$	deformation gradient scaled for volume change.
$\overline{\mathbf{B}} = \overline{\mathbf{F}}\,\overline{\mathbf{F}}^T$	left Cauchy Green strain tensor.
$\bar{I}_1 = tr(\overline{\mathbf{B}})$	first strain invariant (adjusted for volume).
$\bar{I}_2 = \dfrac{1}{2}\left(\left(\bar{I}_1^2\right) - tr\left(\overline{\mathbf{B}}\,\overline{\mathbf{B}}\right)\right)$	second strain invariant (adjusted for volume).
$d\mathbf{u}$	displacement.
$d\mathbf{L} = \dfrac{\partial d\mathbf{u}}{\partial \mathbf{x}}$	gradient of displacement.
$d\mathbf{D} = \dfrac{1}{2}\left(d\mathbf{L} + d\mathbf{L}^T\right)$	rate of deformation.
$d\mathbf{D}_\mathbf{v}$	rate of deformation computed using virtual displacement $d\mathbf{v}$.
$\mathbf{A} : \mathbf{B}$	scalar product of matrices $\mathbf{A}$ and $\mathbf{B}$.
$de^{vol} = \mathbf{I} : d\mathbf{D}$	volumetric strain rate.
$d\mathbf{e} = d\mathbf{D} - \dfrac{1}{3}de^{vol}\mathbf{I}$	deviatoric strain rate.
$p = -\dfrac{1}{3}\mathbf{I} : \mathbf{s}$	pressure stress (hydrostatic).